OPEN ACCESS

Applied Physics Express 11, 053002 (2018)

https://doi.org/10.7567/APEX.11.053002

Spin-wave wavelength down-conversion at thickness steps

Johannes Stigloher[1], Takuya Taniguchi[2], Marco Madami[3], Martin Decker[1], Helmut S. Körner[1], Takahiro Moriyama[2], Gianluca Gubbiotti[4], Teruo Ono[2,5], and Christian H. Back[1]

[1]*Department of Physics, Regensburg University, 93053 Regensburg, Germany*
[2]*Institute for Chemical Research, Kyoto University, Uji, Kyoto 611-0011, Japan*
[3]*Dipartimento di Fisica e Geologia, Università di Perugia, I-06123 Perugia, Italy*
[4]*Istituto Officina dei Materiali del Consiglio Nazionale delle Ricerche (IOM-CNR), Sede di Perugia, c/o Dipartimento di Fisica e Geologia, I-06123 Perugia, Italy*
[5]*Center for Spintronics Research Network (CSRN), Graduate School of Engineering Science, Osaka University, Toyonaka, Osaka 560-0043, Japan*

Received February 7, 2018; accepted March 12, 2018; published online April 3, 2018

We report a systematic experimental study on the refraction and reflection of magnetostatic spin-waves at a thickness step between two Permalloy films of different thickness. The transmitted spin-waves for the transition from a thick film to a thin film have a higher wave vector compared to the incoming waves. Consequently, such systems may find use as passive wavelength transformers in magnonic networks. We investigate the spin-wave transmission behavior by studying the influence of the external magnetic field, incident angle, and thickness ratio of the films using time-resolved scanning Kerr microscopy and micro-focused Brillouin light scattering. © 2018 The Japan Society of Applied Physics

The manipulation of spin-waves belongs to the research area of magnonics, which aims at the technological utilization of spin-waves,[1,2] and has witnesses increased interest in recent years. Eventually, spin-waves or magnons might be used as building blocks of next-generation computation devices for transferring and processing information.[3] Their advantages include low-power dissipation, potentially small wavelengths in the range of tens of nanometers, and high frequencies in the terahertz regime. However, the targeted generation of coherent spin-waves with small wavelengths is challenging because the standard method of generating spin waves employs microwave antennas whose dimensions limit the wavelength. Overcoming this limit constitute a research field of its own: Demidov et al. decreased the width of a spin-wave wave guide, thus changing the internal field, and subsequently reduced the spin-wave wavelength.[4] Yu et al. made use of the "grating-coupler effect," where an array of ferromagnetic disks is structured on top of an insulating ferrimagnetic yttrium iron garnet (YIG) film.[5,6] Here, modes that match the periodicity of these arrays are resonantly enhanced in excitation efficiency. Approaches that circumvent the use of an antenna include spin torque nano-oscillators,[7,8] the use of magnetic textures such as vortices[9] and domain walls,[10,11] and the generation of spin-waves via multiferroics.[12]

Recently, there have been a series of publications dedicated to the use of a thickness step to change the dispersion relation of spin-waves.[13,14] The natural refraction occurring at the interface can be used to manipulate the spin-wave wavelength[15,16] or focus the spin-wave intensity.[17]

Herein, we present a thorough study of the refraction process of spin-waves at such step interfaces. We emphasize the seamless conversion of the wavelength, i.e., the possibility to reach any desired smaller wave vector in the dipolar dominated range. In addition, we show that this process is easily tunable: We systematically change the structural properties of the process — thickness and incident angle — as well as the magnitude of the external field.

To image the refraction process, we mainly use time-resolved scanning Kerr microscopy (TR-MOKE). Similar to,[13] additional measurements are performed using the phase-resolved micro-focused Brillouin light scattering technique (μ-BLS).[18]

We prepare a series of samples that feature three different thin-film thicknesses d_{thin} (10, 15, and 20 nm). From these samples, each TR-MOKE and μ-BLS experiment is assigned a set. The sample fabrication is performed as follows. First, using radiofrequency (rf) magnetron sputtering, a permalloy (Py) film is deposited with d_{thin} on an intrinsic Si substrate. Second, a region on top is structured via electron beam lithography, Py sputtering, and a lift-off process such that this part has $d_{thick} = 60$ nm. Therefore, an abrupt change of the Py thickness is created, and this thickness step serves as a boundary dividing different media in the experiments. Third, the final sample extents are patterned via electron beam lithography, and with Ar^+ milling, the surrounding Py is removed. Subsequently, SiO_2 (63 nm)/Ti (5 nm)/Au (100 nm) multilayers are sputtered. Finally, an antenna is fabricated from these layers via electron beam lithography and Ar^+ milling. The antenna consists of a 2-μm-width signal line and two 1-μm-width ground lines that are separated from the signal line by 1 μm. This corresponds to a ground-to-ground distance of 5 μm. A sketch of the final sample geometry can be found in Fig. 1(a).

In all the measurements, we direct a microwave current with a frequency of $f = 8$ GHz through the structure, unless otherwise specified. The resulting dynamic Oersted field excites propagating spin-waves with k-vectors perpendicular to the antenna. By changing the orientation of the antenna at an angle θ_{in} to the interface, the initial wave is always incident at θ_{in} to the interface normal. To study the influence of θ_{in} on refraction, we prepare samples featuring three angles (10, 20, and 30°) for every thickness d_{thin}.

The external magnetic field H is always directed along the interface. In all other geometries, static demagnetizing effects occur near the interface, such as tilting of the static magnetization, as well as a reduced internal magnetic field, which alter the spin-wave phase front and are referred to as spin-wave bending. This effect makes the plane wave model unsuitable for fitting the data.

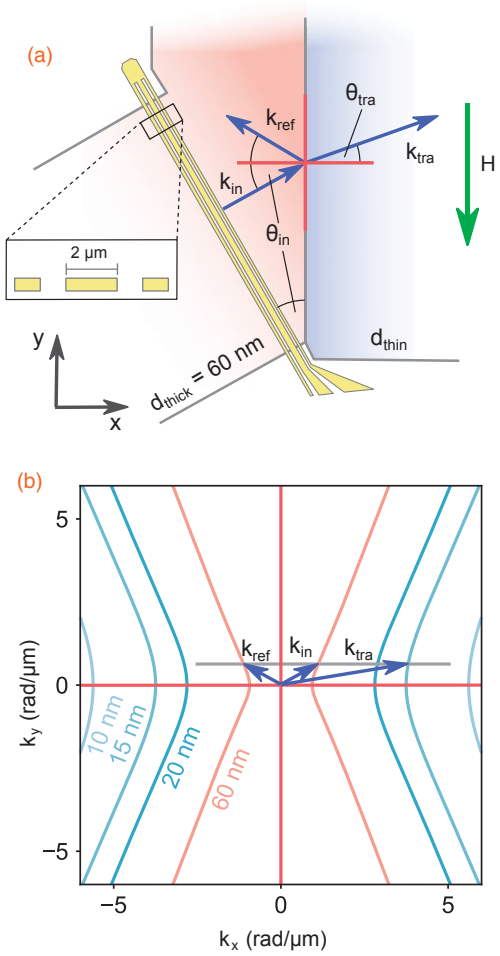

Fig. 1. (a) Sketch of the sample geometry: waves with the wave vector k_{in} impinge onto the interface at θ_{in}, where θ_{in} is determined by the orientation of the patterned antenna, whose dimensions are shown in the inset. The red cross marks the interface and interface normal between the thick (shaded red) and thin (shaded blue) Py films. In (b), the refraction process is shown in the k-space. The cross and arrows are as in (a). Additionally, iso-frequency curves for a frequency of 8 GHz and magnetic field of 45 mT are plotted for the thick (red) and thin (blue) parts. The gray line indicates the conserved k-vector component, and its crossing points with the iso-frequency curves give the refracted and reflected wave vector.

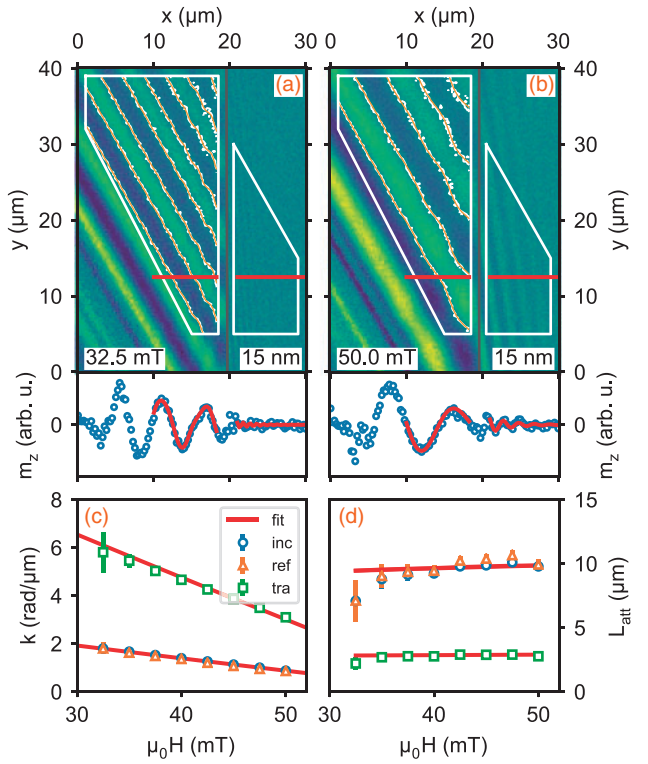

Fig. 2. Panels (a) and (b) show TR-MOKE recorded at 8 GHz data for external magnetic fields of 32.5 and 50 mT, respectively, recorded by TR-MOKE. The black line indicates the interface, and the white boxes are the extent of the area of the fit. The orange lines indicate the zero crossings of the waves, as determined by the fit. Below them, the zero crossings of the data are depicted in white. The antenna is located in the lower left corner and is inclined by 30° towards the interface. Panels (c) and (d) depict the dependence of the wave-vector magnitudes k and the attenuation lengths L_{att} on the external magnetic field. "inc", "ref", and "tra" represent incoming, reflected, and transmitted waves, respectively.

To quantitatively access the refraction process, the iso-frequency curves of the dispersion relation are typically used.[19] These are plotted in Fig. 1(b) for the different thicknesses, a field of 45 mT, and a frequency of 8 GHz. Neglecting the exchange interaction, we directly utilize Eq. (45) in Ref. 20 here and for all quantitative discussions in this paper. With a given incident angle (in this case 30°) one can determine the wave vectors after the refraction process by utilizing Snell's law.[13] Essentially, the wave-vector component along the interface is conserved; thus, the resulting refracted and reflected wave vectors can be derived from crossing points with the appropriate iso-frequency curve.

The dependence of the dispersion relation on the thickness stems from dipolar interactions.[20] This also leads to a dependence of the group velocity on the thickness in this regime. In general, thicker samples feature higher velocities and therefore better propagation.

A simple method of changing the wavelength of spin-waves is to modify the dispersion relation by changing the magnitude of the external magnetic field. Sample images for two different fields are shown in Figs. 2(a) and 2(b) for external fields of 32.5 and 50 mT. The nominal thickness of the thin film is $d_{thin} = 15$ nm, and the incident angle is 30°. In the following discussion, we use these field-sweeps to characterize our samples.

We access the spin-wave characteristics by employing a two-dimensional (2D) fit. The thick part is fitted with a superposition of two plane waves, and the thin part is a simple plane wave. Two waves are necessary to describe the incoming and reflected waves in the thicker film. The area of the fit includes two white boxes: one for the thin part and one for the thick part. In addition, we marked the zero crossings between crests and troughs of the dynamic magnetization in the data (white) and fit (orange). This gives an observable indication of the quality of the fit. We use Snell's law for spin-waves by fixing the tangential component of the k-vector directly in the fit for all three waves. For the same reasons, the attenuation length (the inverse of the imaginary part of the wave vector) along the interface is also fixed. The bottom panels of Figs. 2(a) and 2(b) show line scans along the red lines in the images and the corresponding fits. As shown, a single line scan is not enough to fit the spin-wave in the thin part in Fig. 2(a), as the signal is significantly weaker than in the thick part. Nevertheless, the 2D fit converges to a solution, as it averages over a lager area.

In our wave-vector regime, the wave vector exhibits a linear dependence on H, as shown in Fig. 2(c). The reflected wave almost perfectly matches the wave-vector magnitude of the incoming wave, because the angle of the external field with respect to the propagation direction is equal in both cases. This field sweep can be used to obtain an implicit fit to the dispersion relation $f(k)$ of the lowest spin-wave mode in the dipolar regime. With a fixed gyromagnetic ratio $\gamma = 185$ GHz/T, we retain the parameters of the saturation magnetization $\mu_0 M_S = 1.02 \pm 0.01$ T, $d_{thick} = 62 \pm 2$ nm, and $d_{thin} = 14 \pm 1$ nm by using a single set of parameters for incoming, reflected, and refracted wave.

Figure 2(d) shows the field dependence of the attenuation length

$$L_{att} = v_g \tau = \frac{v_g}{\alpha \gamma \mu_0 \cdot \left(H + \frac{M_S}{2} \right)}$$

with the decay time τ, the damping parameter α, and the group velocity v_g, which can easily be derived as $v_g = 2\pi(\partial f/\partial k)$. We use the parameters obtained for the field dependence of the wave vector. Again, the data for all three waves are used to fit to a single parameter $\alpha = 0.0074 \pm 0.0002$. The result is a rather flat dependence of the attenuation length on the external field, as H is significantly smaller than $M_S/2$ in the sum in the denominator and v_g only weakly depends on H. We verified that the dependence of τ on the direction of the static magnetization[21] does not significantly change the outcome of the fit.

Figure 3 shows the experimental data on the thickness dependence of the wave refraction. The data for Figs. 3(a) and 3(b) are taken at an incidence angle of 30° and an external field of 42.5 mT. The legend and colors are the same as in Fig. 2 but now include BLS data. Other incident angles show qualitatively similar behaviors. For the measurements of the thickness dependence, the magnitude of the external magnetic field is chosen, such that the efficiency of spin-wave excitation by the antenna is maximized for the fixed frequency value of $f = 8.0$ GHz. Essentially, the k-vector dictated by the dispersion relation should roughly match the k-vector of the antenna, i.e., 2π divided by the ground-to-ground distance of the antenna (5 µm). Here, the efficiency of excitation reaches a maximum. We emphasize that we find a wavelength reduction to approximately 0.8 µm for the nominal thickness ratio of 6. Deviations of the BLS data with respect to TR-MOKE stem from slightly different values of both the rf (8.1 GHz) and the external field intensity (45 mT). Within the error, the slightly increased wave vector can be understood by this and by slightly differing sample thicknesses of a few percent.

Figure 3(d) plots the transmission coefficient T, which is defined as the amplitude ratio of transmitted versus incoming wave at the interface. As reported in Ref. 13, the transmission ratio can exceed $T = 1$. However, for lower thicknesses of the thin film, the transmission ratio decreases.

From the combined data presented here and in Ref. 13, we expect a particular thickness ratio that maximizes T. A theory that predicts T is desirable for effectively calculating this *sweet spot* of thickness ratios for the refraction process. The complicated part in formulating such a (quasi)analytical theory is the three-dimensionality of the problem: in addition to the obvious dependence on x and y, in our comparably thick 60 nm film, the surface character of spin-waves already plays

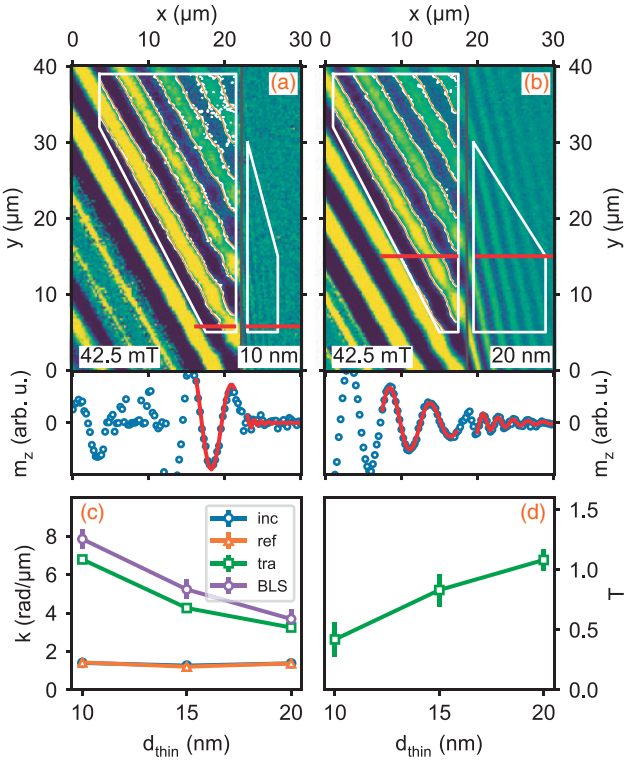

Fig. 3. (a, b) TR-MOKE data recorded at 8 GHz and at an incident angle of 30° for thicknesses of 10 and 20 nm, respectively. (c) Dependence of wave-vector magnitudes k. (d) Transmission coefficient, defined as the amplitude ratio between transmitted and incoming waves at the interface. The color code is clipped in order to facilitate the recognition of the spin-wave in the thin part. Abbreviations are the same as in Fig. 2. "BLS" represents the data recorded by µ-BLS and represents transmitted waves.

an important role.[22] Solving the equations for the dynamic dipolar fields in such a geometry is beyond the scope of this paper. Notable, we have a finite optical penetration depth of roughly 15 nm,[23] which complicates the interpretation of T. For all except the 10 nm film this should be negligible, as we always probe the same top part of the films. Thus, in the case of 10 nm, the value given is underestimated, as less light contributes to the Kerr signal.

The angular dependence for $d_{thin} = 20$ nm is depicted in Fig. 4. The wave-vector magnitudes of incoming and reflected waves shown in Fig. 4(a) decrease with a smaller incident angle, as the dispersion approaches the minimum of k with respect to the angle of the external field. This can be observed on the iso-frequency curve, Fig. 1(b): the minimum of the incoming wave-vector magnitude is reached for a wave traveling along the x-direction ($\theta_{in} = 0°$). This is propagation perpendicular to the static magnetization, i.e., the Damon–Eshbach (DE) configuration, and can also be seen in Fig. 4(b), where the respective attenuation lengths increase when θ_{in} decreases, as the DE geometry also has the highest group velocity. When $\theta_{in} \to 0$, the ratio of transmitted k (k_{tra}) to incoming k (k_{inc}) approaches the ratio of $d_{thick}/d_{thin} = 3$, because the dispersion of DE spin-waves only contains dependencies of $k \cdot d$.[15] The measured deviations from this ratio stem from slight deviations of the thicknesses from the nominal values. In Fig. 4(c), the angles of reflection and refraction are shown in orange and green, respectively. The incoming angle, which is shown in blue, matches the angle of reflection, as the corresponding k-vectors have the same absolute angle with respect

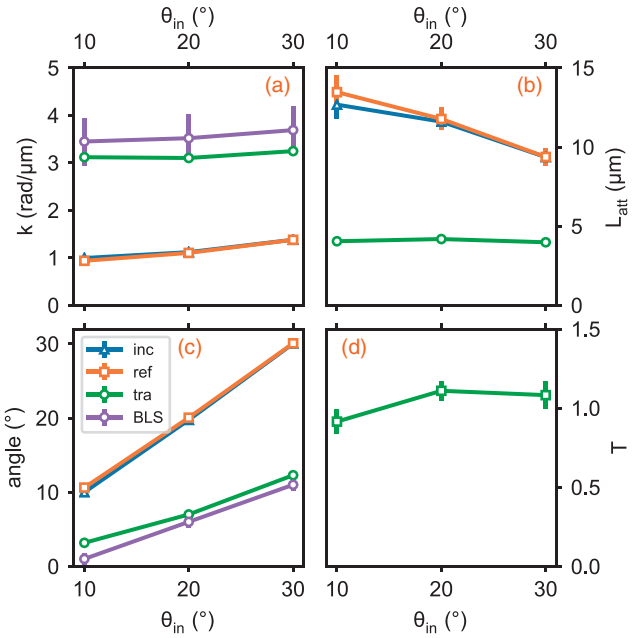

Fig. 4. Angular dependence of (a) the wave-vector magnitudes, (b) the attenuation lengths, (c) the wave vector angles with respect to the interface normal, and (d) the transmission coefficient. The data are recorded at an external field of 42.5 mT and $d_{thin} = 20$ nm. The legend is as in Fig. 3. The violet data reported in panels (a) and (c) are recorded by μ-BLS and correspond to transmitted waves.

to the static magnetization. Figure 4(d) shows the transmission coefficient. Within the error, there is only a small difference between the values obtained at different incident angles. The same holds true for the attenuation length of the transmitted wave shown in Fig. 4(b). As a result, the efficiency of the transmission process seems to be independent of the angle for all angles investigated here.

In conclusion, we investigated the transmission of spin-waves through different thickness steps. To gain insight into the magnetic film properties as well as the refraction process, we also studied the dependence on the external magnetic field and the incident angle, respectively. The increase in the wave vector magnitude scales with the thickness of the film and can be seamlessly tuned to produce a desired wave vector in the sub-micrometer range. The downside for up-conversion of wave vectors is the enhanced wave attenuation, which is mainly due to a reduced group velocity in thinner films. However, the reduced group velocity is a characteristic of the dispersion relation and is therefore shared by all wavelength-conversion techniques that aim to inject waves in such a film.

Antennas with center wave vectors of up to 20 rad/μm have already been demonstrated.[24] As shown in our experiments, a conversion of a factor of 3–4 is achieved with a high transmission efficiency. In this range of wave vectors, the use of a thickness step is attractive from a technological viewpoint, especially because the main alternative — the grating-coupler technique — can reach even lower wavelengths[6] but only allows for conversion efficiencies of approximately 0.2 between fundamental and higher-order modes.[5] Care must be taken when designing devices that feature these large wave vectors. Because when the dispersion is increasingly influenced by the exchange interaction, the k ratio no longer matches the thickness ratio.

1) M. Krawczyk and D. Grundler, J. Phys.: Condens. Matter **26**, 123202 (2014).
2) A. V. Chumak, V. I. Vasyuchka, A. A. Serga, and B. Hillebrands, Nat. Phys. **11**, 453 (2015).
3) G. Csaba, A. Papp, and W. Porod, Phys. Lett. A **381**, 1471 (2017).
4) V. E. Demidov, M. P. Kostylev, K. Rott, J. Münchenberger, G. Reiss, and S. O. Demokritov, Appl. Phys. Lett. **99**, 082507 (2011).
5) H. Yu, G. Duerr, R. Huber, M. Bahr, T. Schwarze, F. Brandl, and D. Grundler, Nat. Commun. **4**, 2702 (2013).
6) H. Yu, O. d Allivy Kelly, V. Cros, R. Bernard, P. Bortolotti, A. Anane, F. Brandl, F. Heimbach, and D. Grundler, Nat. Commun. **7**, 11255 (2016).
7) V. E. Demidov, S. Urazhdin, and S. O. Demokritov, Nat. Mater. **9**, 984 (2010).
8) M. Madami, S. Bonetti, G. Consolo, S. Tacchi, G. Carlotti, G. Gubbiotti, F. B. Mancoff, M. A. Yar, and J. Akerman, Nat. Nanotechnol. **6**, 635 (2011).
9) S. Wintz, V. Tiberkevich, M. Weigand, J. Raabe, J. Lindner, A. Erbe, A. Slavin, and J. Fassbender, Nat. Nanotechnol. **11**, 948 (2016).
10) B. Van de Wiele, S. J. Hämäläinen, P. Balaz, F. Montoncello, and S. van Dijken, Sci. Rep. **6**, 21330 (2016).
11) M. Voto, L. Lopez-Diaz, and E. Martinez, Sci. Rep. **7**, 13559 (2017).
12) S. J. Hämäläinen, F. Brandl, K. J. A. Franke, D. Grundler, and S. van Dijken, Phys. Rev. Appl. **8**, 014020 (2017).
13) J. Stigloher, M. Decker, H. S. Körner, K. Tanabe, T. Moriyama, T. Taniguchi, H. Hata, M. Madami, G. Gubbiotti, K. Kobayashi, T. Ono, and C. H. Back, Phys. Rev. Lett. **117**, 037204 (2016).
14) J. Toedt, S. Mansfeld, D. Mellem, W. Hansen, D. Heitmann, and S. Mendach, Phys. Rev. B **93**, 184416 (2016).
15) K. Tanabe, R. Matsumoto, J. Ohe, S. Murakami, T. Moriyama, D. Chiba, K. Kobayashi, and T. Ono, Appl. Phys. Express **7**, 053001 (2014).
16) H. Hata, T. Moriyama, K. Tanabe, K. Kobayashi, R. Matsumoto, S. Murakami, J. Ohe, D. Chiba, and T. Ono, J. Magn. Soc. Jpn. **39**, 151 (2015).
17) J. Toedt, M. Mundkowski, D. Heitmann, S. Mendach, and W. Hansen, Sci. Rep. **6**, 33169 (2016).
18) M. Madami, G. Gubbiotti, S. Tacchi, and G. Carlotti, in *Solid State Physics*, ed. R. E. Camley and R. L. Stamps (Elsevier, Amsterdam, 2012) Vol. 63, Chap. 2.
19) E. H. Lock, Phys. Usp. **51**, 375 (2008).
20) B. A. Kalinikos and A. N. Slavin, J. Phys. C **19**, 7013 (1986).
21) D. D. Stancil and A. Prabhakar, *Spin Waves: Theory and Application* (Springer, New York, 2009).
22) R. W. Damon and J. R. Eshbach, J. Phys. Chem. Solids **19**, 308 (1961).
23) K. K. Tikuišis, L. Beran, P. Cejpek, K. Uhlířová, J. Hamrle, M. Vaňatka, M. Urbánek, and M. Veis, Mater. Des. **114**, 31 (2017).
24) T. Brächer, M. Fabre, T. Meyer, T. Fischer, S. Auffret, O. Boulle, U. Ebels, P. Pirro, and G. Gaudin, Nano Lett. **17**, 7234 (2017).